Journal of Alloys and Compounds 509 (2011) 4608–4612

Contents lists available at ScienceDirect

Journal of Alloys and Compounds

journal homepage: www.elsevier.com/locate/jallcom

Multiferroic properties of $Bi_{3.15}Nd_{0.85}Ti_3O_{12}$–$CoFe_2O_4$ bilayer films derived by a sol–gel processing

Bin Yang, Zheng Li, Ya Gao, Yuanhua Lin, Ce-Wen Nan*

Department of Materials Science and Engineering, State Key Lab of New Ceramics and Fine Processing, Tsinghua University, Beijing 100084, People's Republic of China

ARTICLE INFO

Article history:
Received 8 October 2010
Received in revised form 12 January 2011
Accepted 19 January 2011
Available online 26 January 2011

Keywords:
Thin films
Composite materials
Sol–gel processes
Ferroelectrics
Magnetic films and multilayers

ABSTRACT

Multiferroic $Bi_{3.15}Nd_{0.85}Ti_3O_{12}$ (BNT)–$CoFe_2O_4$ (CFO) bilayer films with different preferential orientations and thickness fractions for the BNT layer were prepared on Pt/Ti/SiO_2/Si substrate by a sol–gel processing. The experimental results showed that the bilayer films with preferentially *a*-axis oriented and thicker BNT layer have better ferroelectric properties. The magnetoelectric coupling response is weak when the degree of *a*-axis orientation of the BNT layer is low or the leakage current is high, while it is mainly controlled by the thickness fraction in other cases.

1. Introduction

The past few years have seen a tremendous flurry of research interest in multiferroic magnetoelectric (ME) materials that show simultaneous magnetic order and ferroelectric ordering [1–4]. By comparing to the existing single-phase multiferroics, the composite multiferroics exhibit a much larger room-temperature ME effect, namely, the induction of an electric polarization by an external magnetic field and/or vice versa [5,6].

Among the ME composite systems, ME bilayer films of ferroelectric and ferromagnetic layers have undoubtedly shown their great significance since they are less leaky and easy to be on-chip integration [7–9]. Pb-based oxides are generally chosen as the ferroelectric component to achieve high performance [7–17]. The Pb toxicity, however, is a terrible problem. Recent studies have shown that lanthanides-substituted $Bi_4Ti_3O_{12}$ (Ln-BT) is a promising candidate for use in Pb-free ferroelectrics because of its excellent ferroelectric properties [18–20]. However, as far as we know, few multiferroic bilayer films in which Ln-BT is used as the ferroelectric component have been studied [21].

In this work, Nd-substituted BT, i.e., $Bi_{3.15}Nd_{0.85}Ti_3O_{12}$ (BNT), and $CoFe_2O_4$ (CFO) are selected as ferroelectric and magnetic phases for their excellent ferroelectric and magnetic characteristics. The bilayer films with two different preferential orientations (*a*-axis orientation and random orientation) and different thickness fractions for the bottom BNT layer are prepared by a sol–gel processing. Their dependence of the multiferroic properties on the thickness fraction and the preferential orientation of the BNT layer is investigated.

2. Experimental procedures

Multiferroic BNT–CFO bilayer films were fabricated on Pt/Ti/SiO_2/Si substrate with a simple solution method and spin-coating processing. The BNT (0.08 M) and CFO (0.2 M) precursor solutions were prepared via the same processing as reported previously [13,22,23]. The two-step rapid thermal-treatment processing was employed to anneal the bilayer films. That is, the BNT precursor solution was firstly spin-coated onto the substrate and heat treated repeatedly to obtain a BNT thin film with the desired thickness, and then the CFO precursor solution was spin-coated onto the BNT thin film and heat treated repeatedly until the CFO thin film achieved the desired thickness.

The two different preferentially oriented BNT layers were obtained through different rapid heat-treatment processing. The preferentially *a*-axis oriented BNT bottom layers (denoted as *a*-BNT) were obtained when the BNT layer was heat-treated as follows. Each coated BNT layer was heated at 250 °C for 5 min for drying, 450 °C for 5 min for pyrolysis, 650 °C for 2 min for precrystallization, and 750 °C for 2 min for crystallization. The randomly oriented BNT bottom layers (denoted as *r*-BNT) were obtained when each coated BNT layer was dried at 250 °C for 5 min, pyrolysized at 450 °C for another 5 min, and precrystallized at 550 °C for 2 min, and finally all the BNT layers were annealed at 750 °C for 5 min together. The CFO layers were heat-treated as follows. Each coated CFO layer was dried at 200 °C for 5 min, and pyrolysized at 400 °C for 5 min. The spin coating was repeated to achieve the desired thickness, and the final films were annealed at 750 °C for 5 min together.

The BNT (500 nm)–CFO (100 nm) bilayer films with two different preferential orientations, i.e., *a*-BNT–CFO and *r*-BNT–CFO, were obtained through the corresponding method as described above. Multiferroic *x*BNT–(1 − *x*)CFO (*x* = 0.375, 0.5, 0.625, 0.75, 0.875, *x* being the thickness fraction of BNT layer) bilayer films were fabricated via the same method as described in the preparation of the *a*-BNT–CFO bilayer films. The total thickness, *t*, was fixed at about 400 nm.

* Corresponding author. Tel.: +86 10 62773587; fax: +86 10 62771160.
E-mail address: cwnan@mail.tsinghua.edu.cn (C.-W. Nan).

0925-8388/$ – see front matter © 2011 Elsevier B.V. All rights reserved.
doi:10.1016/j.jallcom.2011.01.124

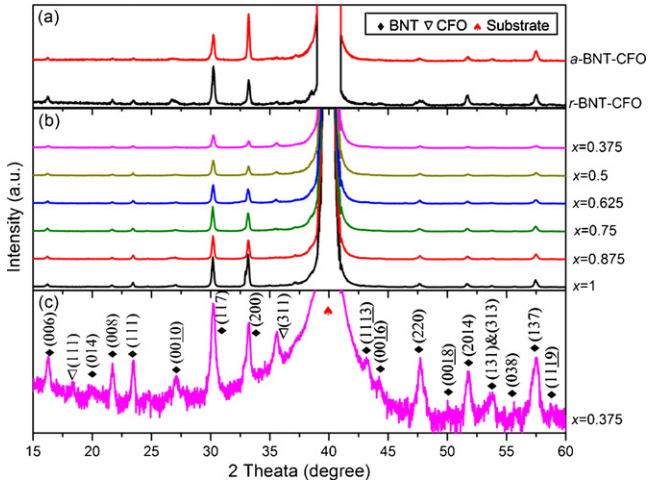

Fig. 1. XRD patterns of (a) *a*-BNT–CFO and *r*-BNT–CFO; (b) *x*BNT–(1 − *x*)CFO bilayer films; and (c) the enlarged plot of the 0.375BNT–0.625CFO bilayer film for clear illustration of the CFO peaks.

The phases in the bilayer films were characterized using X-ray diffraction (XRD) (Rigaku D/max- 3A) with CuKα radiation. A cross-sectional examination was made by scanning electron microscopy (SEM) (Hitachi S5500). For electrical measurement, top Pt electrodes of about 300 μm in diameter were sputtered onto the top film surface to form ferroelectric capacitors. The electric properties of such capacitors were measured by a TF analyzer2000 (aixACCT Co.). Magnetic properties were measured using Physical Property Measurement System (PPMS-9T, Quantum Design Co.). The ME effect was measured in terms of the variation in the induced voltage or polarization by the applied magnetic field. A DC magnetic field which is superimposed by a small AC magnetic field is applied parallel to the sample plane (in-plane mode). The voltage signal generated from the sample induced by the in-plane magnetic field was measured through a lock-in amplifier (SR 850). All measurements were carried out at room temperature.

3. Results and discussion

Fig. 1 shows the XRD patterns of the BNT–CFO bilayer films. Two evident sets of well-defined peaks are observed, and they belong to polycrystalline BNT and CFO, respectively. Neither additional nor intermediate phase is detected, excluding any obvious interreaction between the two oxide phases. The degree of preferential *a*-axis orientation for the BNT layer is estimated as [24]:

$$\alpha_a = \frac{\sum(I_{h00}/I^*_{h00})}{\sum(I_{hkl}/I^*_{hkl})}, \quad (1)$$

where I_{hkl} is the measured intensity of the ($h\,k\,l$) peak for the BNT component of the films, I^*_{hkl} is the intensity for the BNT powder (not shown here). The calculated values of α_a are listed in Table 1, which shows that α_a increase a bit with the thickness fraction, *x*, of the BNT layers for the *x*BNT–(1 − *x*)CFO bilayer films, as observed previously [25].

The cross-sectional SEM images of the BNT–CFO bilayer films are shown in Fig. 2. All the films look dense and similar; the interface between the BNT and CFO layers is clear. The thicknesses of the BNT and CFO layers in the *a*-BNT–CFO and *r*-BNT–CFO bilayer films respectively are about 500 nm and 100 nm, so the thickness fraction of the BNT layer in these two bilayer films is about 0.83. The total film thicknesses of all the *x*BNT–(1 − *x*)CFO bilayer films are about 400 nm. The BNT layer thickness is about 150, 200, 250, 300, and 350 nm for *x* = 0.375, 0.5, 0.625, 0.75, and 0.875, respectively.

The leakage behavior of the bilayer films is shown in Fig. 3. Low leakage means high electric resistivity, as well as dense and good microstructure as shown in Fig. 2. The leakage of the *a*-BNT–CFO bilayer film is higher than that of the *r*-BNT–CFO bilayer films (Fig. 3(a)). It can be attributed to that the Bi_2O_2 layers which influence the insulation performance are parallel to the direction of the applied electric field, and thus can not restrain the leakage current well for the *a*-axis oriented BNT grains [26]. As to the *x*BNT–(1 − *x*)CFO bilayer films, the leakage decreases with the increase in the thickness fraction *x* of the BNT layer as expected (Fig. 3(b)), which is due to much higher resistivity of BNT than CFO.

Three possible leakage current mechanisms are commonly observed in oxide thin films, i.e., Pool–Frenkel emission, Schottky emission and space-charge-limited conduction (SCLC) model [27,28]. These three models yield a different linear dependence of the current density *J* on the voltage *V*, i.e., $\ln(Jd/V) \propto V^{0.5}$ for Pool–Frenkel emission, $\ln(J/T^2) \propto V^{0.5}$ for Schottky emission, and $\log J \propto \log V$ for SCLC model [27], where *d* is the film thickness, and *T* is the temperature (300 K here). So as to find the possible leakage mechanism for the bilayer films, we plotted the leakage data as $\ln(Jd/V)$ *vs* $V^{0.5}$ and $\ln(J/T^2)$ *vs* $V^{0.5}$, (not shown here) as well as $\log J$ *vs* $\log V$ for the *a*-BNT–CFO and *r*-BNT–CFO bilayer films (Fig. 3(a)), and the *x*BNT–(1 − *x*)CFO bilayer films (Fig. 3(b)). The results show the leakage current for the present films is more probably controlled by the SCLC mechanism. The log–log plot can be fitted with two linear segments with different slopes (*s*). At low electric field, the leakage current appears linear with slopes (s_1) near unity, indicating Ohmic conduction. As electric field increases, more electrons can be injected into the films, and thus the bilayer films change to follow SCLC mechanism ($s_2 \geq 2$). The values of s_1 and s_2 are listed in Table 2. It seems that the traps are free or distributed discretely in the single-phase BNT thin film, for its value of s_2 is about 2; while they are distributed within the band gap in the BNT–CFO bilayer films, because their values of s_2 are greater than 2 [28].

Fig. 4 shows the polarization–electric field (*P*–*E*) hysteresis loops of the BNT–CFO bilayer films and the single-phase BNT thin film (*x* = 1). The *a*-BNT–CFO bilayer film shows better ferroelectric behavior (Fig. 4(a)), which confirms that the spontaneous polarization in BNT thin films is mainly along its *a*-axis-orientation. The ferroelectric behavior of the film with *x* = 0.875 almost coincides with that of the single-phase BNT film. Moreover, the loops for *x* = 0.375 and 0.5 show rounded tips, indicating high leakage current (Fig. 3(b)). Almost all the bilayer films demonstrate larger *P*–*E* loops, with higher remnant polarization (P_r) and coercive field (E_c), as shown in Table 3, than those of the single-phase BNT film. The enhancement in both P_r and E_c can be attributed to: (i) the presence of space charges at the BNT–CFO interface [29], and (ii) the reduction of the actual field seen by the BNT layer due to the sharing electric field of the CFO layer.

The typical magnetic hysteresis loops are observed in the BNT–CFO bilayer films, and for comparison, in the single-phase CFO films (*x* = 0), as shown in Fig. 5, measured with the magnetic fields up to 15 kOe applied parallel to the sample plane. All the values are normalized only to the volume of CFO layer. The loop of the *r*-BNT–CFO bilayer film almost coincides with that of the *a*-BNT-CFO bilayer film, so it is not shown for clarity. An enhancement in the saturation magnetization M_s and a decrease in the coercive field H_c are observed for the bilayer films, which could be due to the reduction of tensile stress in CFO layers. As known, the stress σ facilitates the magnetization when the stress σ and magnetostriction λ_s meet $\sigma\lambda_s > 0$, but retards the magnetization when $\sigma\lambda_s < 0$ [30]. So the compressive stress favors the magnetization of CFO layer while the tensile stress does not, since the magnetostriction λ_s of polycrystalline CFO is negative. For the single-phase CFO film, the volume shrinkage occurs during thermal annealing, but the stiff substrate puts off it, and thus the tensile stress is generated in the CFO film [12]. When deposited on the BNT film which can also act as a buffer layer, the CFO film could release the tensile stress, thus the magnetizing is easer for the bilayer films, the magnetization is enhanced, and the coercive field decreases.

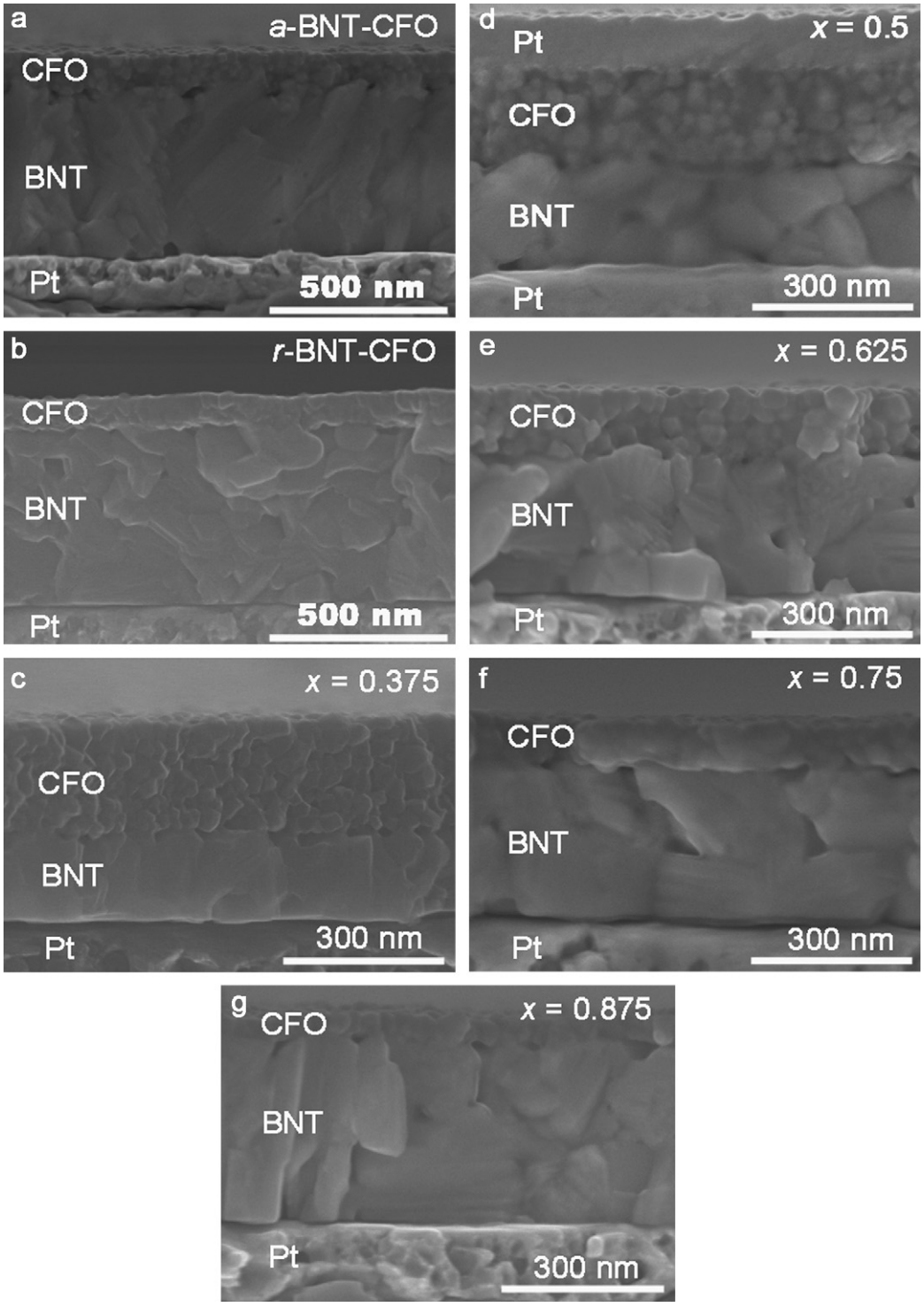

Fig. 2. Cross-sectional SEM images of the BNT–CFO bilayer films.

Table 1
The calculated values of α_a for different BNT–CFO bilayer films.

Films	*a*-BNT–CFO	*r*-BNT–CFO	*x*BNT–(1 − *x*)CFO				
x	0.83	0.83	0.375	0.5	0.625	0.75	0.875
α_a(%)	60	30	31	35	39	40	42

Table 2
The fitted values of s_1 and s_2 for different BNT–CFO bilayer films.

Films	*a*-BNT–CFO	*r*-BNT–CFO	*x*BNT–(1 − *x*)CFO					
x	0.83	0.83	0.375	0.5	0.625	0.75	0.875	1
s_1	1.38	1.38	1.41	1.27	1.40	1.12	1.44	1.08
s_2	2.22	2.23	3.56	3.04	2.93	2.70	2.81	2.08

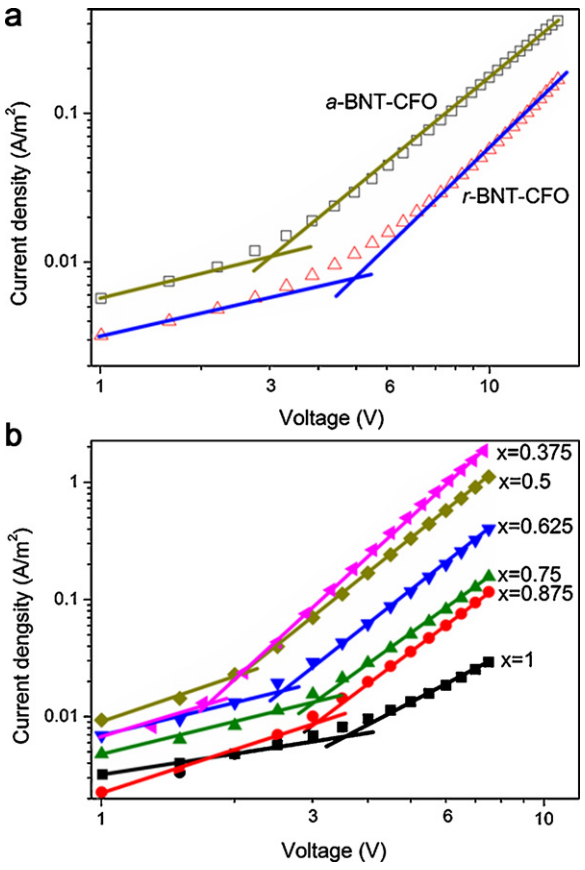

Fig. 3. *J–V* characteristics and the fitted straight lines by the SCLC mechanism of (a) *a*-BNT–CFO and *r*-BNT–CFO; as well as (b) *x*BNT–(1 − *x*)CFO bilayer films.

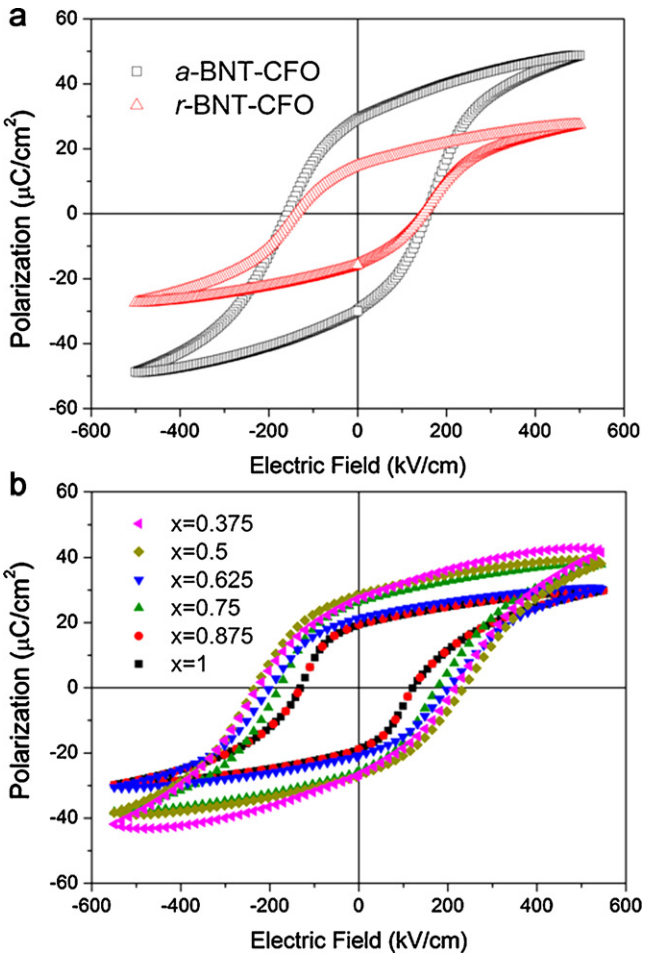

Fig. 4. Polarization–electric field hysteresis loops of (a) *a*-BNT–CFO and *r*-BNT–CFO, as well as (b) *x*BNT–(1 − *x*)CFO bilayer films. The loop of the single-phase BNT film is also shown for comparison.

The existence of a coupling between the magnetic and ferroelectric components is confirmed by the measurement of a ME response voltage signal. A DC magnetic field (H_{DC}), which is superimposed by an AC magnetic field (460 Oe), is applied parallel to the sample plane. The measured ME response voltages induced by the DC + AC magnetic fields are shown in Fig. 6, where the response signals for the 0.375BNT–0.625CFO bilayer film are too weak to be observed. As seen, the values of the ME voltage ΔV [$\Delta V = V(H_{DC}) - V(H_{DC} = 0)$] induced purely by the in-plane bias DC magnetic field H_{DC} are about 5 μV for the 0.875BNT–0.125CFO sample. This ME voltage response is a bit higher than those observed in the $Pb(Zr_{0.52}Ti_{0.48})O_3$–CFO bilayer films [7,12], but above two orders of magnitude lower than that of the bulk ME laminated $Pb(Zr,Ti)O_3$-ferrite ceramics [31], mainly due to the clamping effect from the substrate [3]. The ME response signals increase with the DC magnetic field firstly, and then tend to saturate, which basically follows the change tendency of the magnetostriction of CFO with increasing DC magnetic field, confirming the interfacial strain-mediated ME coupling.

Many factors may affect the ME coupling in bilayer films, such as interface, thickness fraction and orientation of the components [7,12], leakage current, and so on. Based on Figs. 3 and 6, it seems that the ME response signals are weak when the leakage current is high or the degree of preferential *a*-axis orientation, α_a, is low; while they are obvious and dominated by the thickness fraction of the BNT layer in other cases. For the *r*-BNT–CFO bilayer film, its value of α_a is the lowest (30%), the ferroelectric property of the BNT layer is not good enough (Fig. 4(a) and Table 3) to respond well to the transferred strain from the CFO layer, and thus its ME coupling

Table 3
The values of the remnant polarization (P_r) and coercive field (E_c) of the BNT–CFO bilayer films.

Films	*a*-BNT–CFO	*r*-BNT–CFO	*x*BNT–(1 − *x*)CFO					
x	0.83	0.83	0.375	0.5	0.625	0.75	0.875	1
P_r (μC cm^{-2})	29.2	14.8	27.5	28.6	21.5	26.3	19.4	19.4
E_c (kV cm^{-1})	156	147	216	235	202	176	121	121

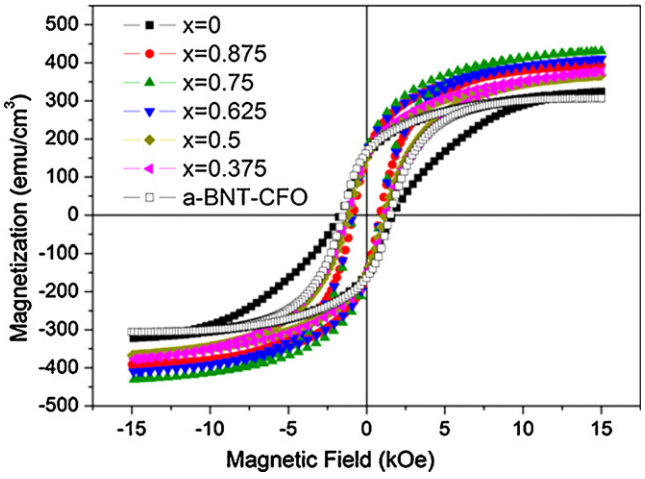

Fig. 5. The in-plane *M*–*H* hysteresis loops of the BNT–CFO bilayer films bilayer films. The loop of the single-phase CFO thin film is also shown for comparison.

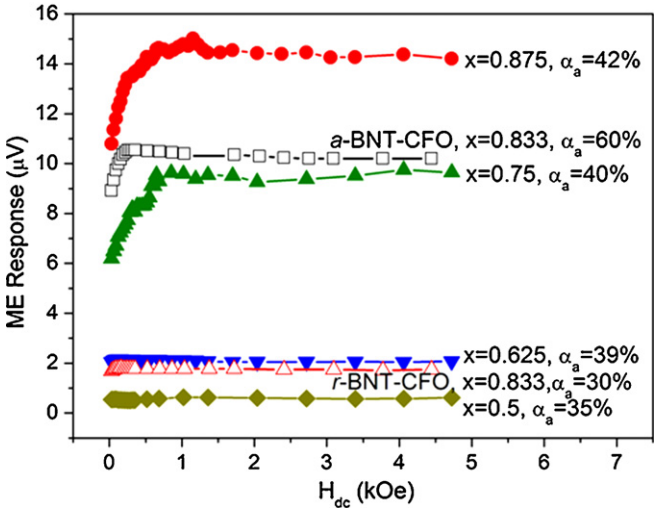

Fig. 6. The ME response voltage signals of the BNT–CFO bilayer films.

is weak. For the 0.5BNT–0.5CFO and 0.625BNT–0.375CFO bilayer films, the high leakage current causes the low ME response voltages. As to the 0.375BNT–0.625CFO bilayer film, both the low α_a and the high leakage current lead to the unobservable ME response signals. While in other cases, the ME response voltages seems to increase with the thickness fraction x of the BNT layer, so the *a*-BNT–CFO bilayer film has a bit weaker signals than the 0.875BNT–0.125CFO bilayer film, even though its value of α_a is higher. The single-phase BNT film ($x = 1$) does not show any ME signal as expected. Therefore, there might be a value of x between 0.875 and 1, at which the ME response is the maximal. It should be noted that the ME response signals of the *r*-BNT–CFO bilayer films are unexpectedly weak. As to the BNT films, the piezoelectric coefficient (d_{33}) ratio in *a*-axis and random orientations is only about 1.5 [19]. Therefore, there should be other factors that influence the ME coupling in the bilayer films, such as interface defects, grain size, grain boundaries, and so on. These remain to be clarified.

4. Conclusions

In summary, the multiferroic BNT–CFO bilayer films with different preferential orientations and thickness fractions for the BNT layer have been obtained by a sol–gel processing. The preferential orientation and the thickness fraction, as well as the leakage current have obvious effect on their properties. The bilayer films with preferentially *a*-axis oriented and thicker BNT layer show better ferroelectric properties. The ME coupling response is weak when the degree of preferential *a*-axis orientation for the BNT layer is low or the leakage current is high, while it increases with the thickness fraction of the BNT layer in other cases.

Acknowledgements

This work was supported by the NSF of China (grant nos. 50921061 and 50832003) and the National Basic Research Program of China (973-Program, grant no. 2009CB623303).

References

[1] W. Eerenstein, N.D. Mathur, J.F. Scott, Nature 442 (2006) 759–765.
[2] M. Fiebig, J. Phys. D 38 (2005) R123–R152.
[3] C.W. Nan, M.I. Bichurin, S.X. Dong, D. Viehland, G. Srinivasan, J. Appl. Phys. 103 (2008) 031101.
[4] R. Ramesh, N.A. Spaldin, Nat. Mater. 6 (2007) 21–29.
[5] D. Khomskii, Physics 2 (2009) 20–28.
[6] W. Prellier, M.P. Singh, P. Murugavel, J. Appl. Phys. 17 (2005) R803–R832.
[7] H.C. He, J. Ma, J. Wang, C.W. Nan, J. Appl. Phys. 103 (2008) 034103.
[8] Y.J. Wu, J.G. Wan, J.M. Liu, G.H. Wang, Appl. Phys. Lett. 96 (2010) 152902.
[9] Y. Zhang, J. Liu, X.H. Xiao, T.C. Peng, C.Z. Jiang, Y.H. Lin, C.W. Nan, J. Phys. D 43 (2010) 082002.
[10] W. Chen, W.G. Zhu, X.F. Chen, Z.H. Wang, J. Am. Ceram. Soc. 93 (2010) 796–799.
[11] S. Dussan, A. Kumar, J.F. Scott, R.S. Katiyar, Appl. Phys. Lett. 96 (2010) 072904.
[12] H.C. He, J. Ma, Y.H. Lin, C.W. Nan, J. Appl. Phys. 104 (2008) 114114.
[13] H.C. He, J. Wang, B.P. Zhou, C.W. Nan, Adv. Funct. Mater. 17 (2007) 1333–1338.
[14] Z. Li, Y. Wang, Y.H. Lin, C. Nan, Phys. Rev. B 79 (2009) 180406.
[15] C.H. Sim, A.Z.Z. Pan, J. Wang, J. Appl. Phys. 103 (2008) 124109.
[16] C.A.F. Vaz, J. Hoffman, Y. Segal, J.W. Reiner, R.D. Grober, Z. Zhang, C.H. Ahn, F.J. Walker, Phys. Rev. Lett. 104 (2010) 127202.
[17] J.X. Zhang, J.Y. Dai, H.L.W. Chan, J. Appl. Phys. 107 (2010) 104105.
[18] G.D. Hu, J. Appl. Phys. 100 (2006) 096109.
[19] H. Maiwa, N. Iizawa, D. Togawa, T. Hayashi, W. Sakamoto, M. Yamada, S. Hirano, Appl. Phys. Lett. 82 (2003) 1760–1762.
[20] Y. Qiao, C.J. Lu, Y.J. Qi, Y.H. Zhou, Physica B 403 (2008) 2488–2494.
[21] Z.X. Cheng, X.L. Wang, C.V. Kannan, K. Ozawa, H. Kimura, T. Nishida, S.J. Zhang, T.R. Shrout, Appl. Phys. Lett. 88 (2006) 132909.
[22] B. Yang, D.M. Zhang, B. Zhou, L.H. Huang, C.D. Zheng, Y.Y. Wu, D.Y. Guo, J. Yu, J. Cryst. Growth 310 (2008) 4511–4515.
[23] J. Yu, Y. Bin, J. Li, X.M. Liu, C.D. Zheng, Y.Y. Wu, D.Y. Guo, D.M. Zhang, J. Phys. D 41 (2008) 035304.
[24] C.J. Lu, Y. Qiao, Y.J. Qi, X.Q. Chen, J.S. Zhu, Appl. Phys. Lett. 87 (2005) 222901.
[25] L.L. Jiao, Z.M. Liu, G.D. Hu, S.G. Cui, Z.J. Jin, Q. Wang, W.B. Wu, C.H. Yang, J. Am. Ceram. Soc. 92 (2009) 1556–1559.
[26] R.H. Shin, J.H. Lee, G. Kim, W. Jo, O.J. Kwon, C. Park, D.H. Kim, H.J. Lee, J. Kang, Jpn. J. Appl. Phys. 48 (2009) 111407–111412.
[27] G.W. Pabst, L.W. Martin, Y.H. Chu, R. Ramesh, Appl. Phys. Lett. 90 (2007) 072902.
[28] P. Zubko, D.J. Jung, J.F. Scott, J. Appl. Phys. 100 (2008) 114113.
[29] L. Baudry, J. Appl. Phys. 86 (1999) 1096–1101.
[30] R.C.O. Handley, Modern Magnetic Materials: Principles and Applications, Chemical Industry, Beijing, 2002.
[31] J. Zhai, N. Cai, Z. Shi, Y.H. Lin, C.W. Nan, J. Appl. Phys. 95 (2004) 5685–5687.